Roundoff Noise Analysis for Digital Signal Power Processors Using Welch's Power Spectrum Estimation

CHONG-YUNG CHI, DAVID LONG, AND FUK-KWOK LI

Abstract—**In this paper, we present an analysis for the noise due to finite word length effects for digital signal power processors using Welch's power spectrum estimation technique to measure the power of Gaussian random signals over a frequency band of interest. The input of the digital signal processor contains a finite-length time interval in which the true Gaussian signal is contaminated by Gaussian noise. We analytically derive the roundoff noise-to-signal ratio in the measurement of the signal power. We also present computer simulations which validate the analytical results. These results can be used in tradeoff studies of hardware design such as number of bits required at each processing stage. The results presented in this paper are currently being used in the design of a digital Doppler processor [1], [2] for a radar scatterometer [3]–[5].**

I. Introduction

In Chi, Long, and Li [1], we presented a statistical analysis for the accuracies in the radar backscatter measurements for the NASA Scatterometer (NSCAT) which utilizes a digital Doppler processor (DDP). The reader is referred to [1] for details of the DDP design and general features associated with NSCAT. Briefly, the DDP is a fast Fourier transform (FFT)-based digital signal processor that performs a Welch's power spectrum estimation on the radar return signal (see Fig. 1).

We would like to present the DDP in a more general manner such that its application is not limited to the radar area. Therefore, we will refer to it as a digital signal power processor (DSPP) instead. In [1], the normalized standard deviation of the measurements by the DSPP (the so-called K_p parameter) was derived. However, that derivation assumed that the roundoff noise of the DSPP was negligible. In practical design, roundoff noise is always present and can potentially contaminate the true signal power measurements. In this paper, a roundoff noise analysis of the DSPP is presented. The derived analytical results have been used in tradeoff studies of hardware design such as the number of bits required at each stage of processing to keep the roundoff noise-to-signal ratio satisfactorily low. Although this derivation was motivated by radar system design, we believe the approach and the results will be helpful in the design of other digital signal processors for estimating the power of random signals.

Manuscript received April 18, 1986; revised January 9, 1987. This work was supported by a contract with the National Aeronautics and Space Administration.

The authors are with the Jet Propulsion Laboratory, California Institute of Technology, Pasadena, CA 91109.

IEEE Log Number 8714129.

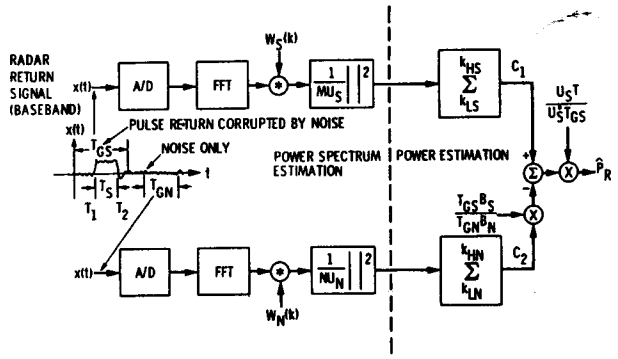

Fig. 1. Signal processing system for a digital signal power processor (DSPP) using Welch's power spectrum estimation.

In Section II, the DSPP based on the Welch's power spectrum estimation and the associated equation for evaluating K_p are summarized. The roundoff noise model that we have used for the DSPP is presented in Section III. The roundoff noise-to-signal ratio is derived in Section IV, and some computer simulations to validate our theoretical results are shown in Section V. We discuss how to use the derived results in the design of the DSPP and draw some conclusions in Section VI.

II. A DSPP Based on Welch's Power Spectrum Estimation

The DSPP is designed to compute an unbiased estimate of the signal power over a frequency band of interest. Essentially, the signal processing procedure employed in the DSPP consists of power spectrum density (psd) estimation and signal power computation. The DSPP based on Welch's power spectrum estimation is shown in Fig. 1. It consists of a) computation of the FFT, b) application of a window by convolution, c) squaring for power detection, and d) computation of the signal power. The input of the DSPP consists of a finite-time-length signal is contaminated by noise. The Welch's power spectrum estimate of the input is first determined, and then the signal-plus-noise power is obtained by summing the estimated periodogram over the desired frequency range. Similarly, an estimate of the noise-only power is computed. The

final estimate of the signal power is obtained by linearly combining these two measurements.

Assume that we are given N_{PS} independent signal-plus-noise pulses and N_{PN} noise-only pulses. For each independent pulse, we assume the following.

(A1) For the noise-only case, the input signal $x(t)$ consists of the thermal noise $n(t)$ which is assumed to be zero-mean Gaussian with psd

$$P_N(f) = b' \quad \text{for} \quad |f| < \frac{f_S}{2} \tag{1}$$

where f_S is the Nyquist sampling frequency. For the signal-plus-noise case, $x(t)$ consists of not only $n(t)$ but also the true return signal $s(t)$ which is assumed to zero-mean Gaussian with psd

$$P_S(f) = \frac{P_R}{B_S} \quad \text{for} \quad f_L \le f \le f_L + B_S = f_H \tag{2}$$

where $2P_R$ is the signal power of $s(t)$ over the frequency range (f_L, f_H) because $P_S(f)$ is a real even nonnegative function of f. Notice that the psd of $s(t)$ outside the interval (f_L, f_H) is not defined explicitly since we are not interested in that region. Also note, from Fig. 1, that the true signal pulse $s(t)$ may be shorter than the input $x(t)$. In [1], we developed an unbiased estimate $\hat{P}_R$ of P_R based on the assumption (A1) and the additional assumption

(A2) The window spectrum $W_S(k)$ is very narrow. By simply extending the result in [1] for multiple independent measurement pulses, the unbiased estimate $\hat{P}_R$ is given by

$$\hat{P}_R = \frac{U_S T}{U_S^* T_{GS}} \left(C_1 - \frac{T_{GS} B_S}{T_{GN} B_N} C_2 \right) \tag{3}$$

where

$$C_1 = \frac{1}{K_S N_{PS} M U_S} \sum_{j=1}^{N_{PS}} \sum_{i=1}^{K_S} \sum_{k=k_{LS}}^{k_{HS}} \left| X_i^{(j)}(k) * W_S(k) \right|^2 \tag{4}$$

and

$$C_2 = \frac{1}{K_N N_{PN} N U_N} \sum_{j=1}^{N_{PN}} \sum_{i=1}^{K_N} \sum_{k=k_{LN}}^{k_{HN}} \left| X_i^{(j)}(k) * W_N(k) \right|^2 \tag{5}$$

where $*$ indicates circular convolution, and C_1 is associated with the power of the signal-plus-noise case, and C_2 is associated with the power of the noise-only case. All the parameters in (3), (4), and (5) are described in Table I (also see [1]). Note that $X_i^{(j)}(k)$ in (4) indicates the Fourier transform of the ith data segment $x_i^{(j)}(n)$ associated with the jth pulse for the signal-plus-noise case. $X_i^{(j)}(k)$ in (5) is then associated with the noise-only case. The ith case segment associated with an input digital signal $x(n)$ is defined as

TABLE I
K_p PARAMETERS

Signal plus noise	Noise only	Description
T_{GS}	T_{GN}	Time interval of one data segment
B_S	B_N	Bandwidth
k_{LS}	k_{LN}	Lower frequency bin number
k_{HS}	k_{HN}	Upper frequency bin number
k_S	k_N	$k_{HS} - k_{LS} + 1$, $k_{HN} - k_{LN} + 1$
$w_S(n)$	$w_N(n)$	Window function (in time domain)
U_S	U_N	$U_S = \frac{1}{M}\sum_{n=0}^{M-1} w_S^2(n)$, $U_N = \frac{1}{N}\sum_{n=0}^{N-1} w_N^2(n)$
N_{PS}	N_{PN}	Number of measurement pulses
K_S	K_N	Number of data segments
M	N	Number of data points per segment $T_{GS}/T, T_{GN}/T$
D		Number of nonoverlapping data points in consecutive data segments
T		Sampling interval = $1/f_S$
T_1		Signal start time
T_S		Signal pulse length
SNR		Signal-to-Noise ratio=$P_r/(B_S b')$
$W_S(q,k)$		Fourier transform of $w_S(n)w_S(n+qD)$
$W_N(q,k)$		Fourier transform of $w_N(n)w_N(n+qD)$
$\gamma_i(n)$		$\begin{cases} rect(nT + (i-1)DT - T_1)w_S(n), & \text{if } 0 \le n \le M-1; \\ 0, & \text{otherwise} \end{cases}$
$\gamma_{ij}(n)$		$\gamma_i(n)\gamma_j(n+(i-j)D)$
$\Gamma_{ij}(k)$		Fourier transform of $\gamma_{ij}(n)$
U_i		$\frac{1}{M}\sum_{n=0}^{M-1}\gamma_i^2(n)$
U_S^*		$\frac{1}{K_S}\sum_{i=1}^{K_S} U_i$
$rect(t)$		$\begin{cases} 1, & 0 \le t \le T_S; \\ 0, & \text{otherwise} \end{cases}$

$$x_i(n) = \begin{cases} x(n + (i-1)D), & \text{if } 0 \le n \le M-1; \\ 0, & \text{otherwise.} \end{cases} \tag{6}$$

Throughout this paper we use $X(k)$ to denote the Fourier transform of $x(n)$. The normalized standard deviation K_p of $\hat{P}_R$ is defined as

$$K_p = \frac{\{\text{Var}[\hat{P}_R]\}^{1/2}}{P_R} \tag{7a}$$

which has been shown in [1] to be

$$K_p = \frac{1}{\sqrt{T_{GS}B_S}} \frac{1}{MU_S^*} \left\{ \frac{1}{K_S^2 N_{PS}} \sum_{k=-k_S}^{k_S} \sum_{i=1}^{K_S} \sum_{j=1}^{K_S} \left(1 - \frac{|k|}{K_S}\right) \left| \Gamma_{ij}(k) + \frac{1}{\text{SNR}} W_S(i-j,k) \right|^2 \right.$$
$$+ \frac{1}{K_N N_{PN}} \frac{T_{GS}B_S}{T_{GN}B_N} \left(\frac{MU_S}{NU_N}\right)^2$$
$$\left. \frac{1}{(\text{SNR})^2} \left[\sum_{k=-k_N}^{k_N} \sum_{q=-K_N}^{K_N} \left(1 - \frac{|k|}{k_N}\right)\left(1 - \frac{|q|}{K_N}\right) \cdot \left| W_N(q,k) \right|^2 \right] \right\}^{1/2} \tag{7b}$$

where all the parameters are described in Table I.

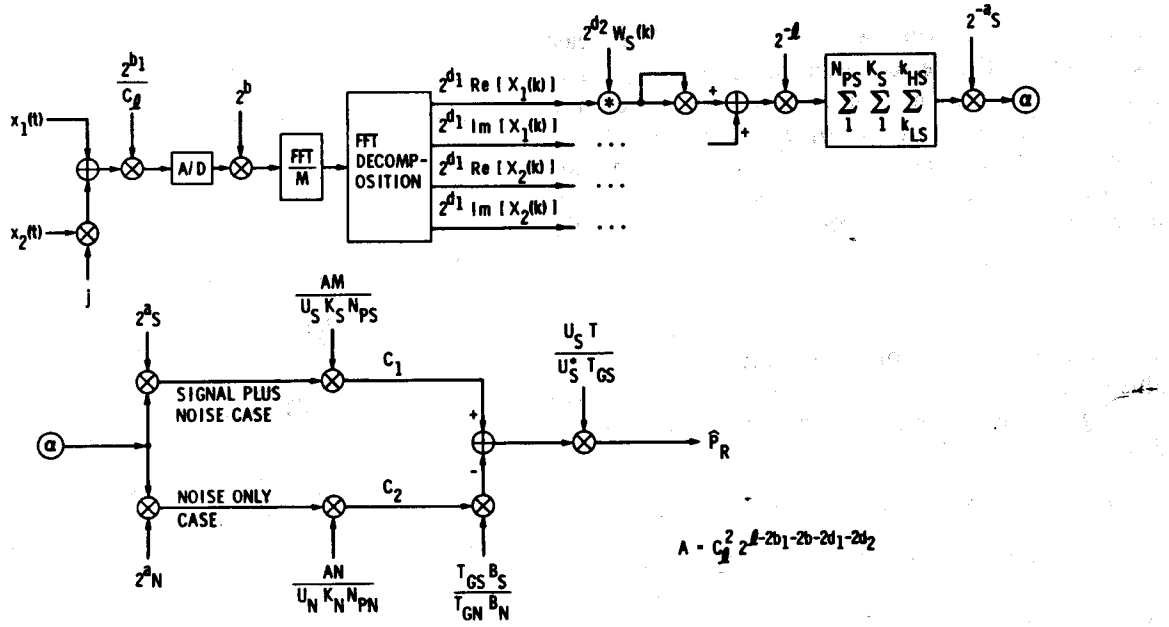

Fig. 2. A realization of the DSPP using Welch's power spectrum estimation.

A practical consideration in the implementation of a digital signal processor is the limitation in the word length at each stage of processing. The power of roundoff noise in the output due to finite word length effects depends on the realization of the digital signal processor. The realization will be driven by the dynamic range at each stage, computation speed limitations, etc. For example, the design of the DDP in NSCAT requires that the digital processor have a dynamic range to process input signal with the SNR range from -20 dB to $+26$ dB. The SNR range in the input signal determines the dynamic range at each stage of the digital processor, and hence, the number of bits at each stage to prevent overflow. In order to minimize the number of bits at each stage, some of the least significant bits would have to be discarded between stages. The roundoff noise accumulated in the output will increase as a function of the discarded bits.

Another practical consideration is the use of fixed-point arithmetic. When all processing is done with fixed-point arithmetic, bit-shifting may be performed at each stage to keep the digital number within a proper dynamic range such that overflow and underflow are minimized. One bit shifted to the left is equivalent to multiplication by 2. One bit shifted to the right is equivalent to multiplication by $1/2$ or the truncation of a least significant bit. During computation of the FFT with radix 2 which is used in the presented DSPP in this paper, a bit-shift right before each stage of the FFT may be performed in order to prevent FFT overflow. Thus, the scale factor $1/M$ will be included within FFT. Also, other artificial scale factors may be introduced to avoid overflow or to simplify the hardware design.

In implementing the DSPP, a number of digital signal processing techniques can be used to minimize the number of arithmetic operations. For example, when computing FFT's of real signals we can perform two FFT computations simultaneously as follows. The Fourier transforms $X_1(k)$ and $X_2(k)$ of two real signals $x_1(n)$ and $x_2(n)$ can be obtained by

$$X_1(k) = \frac{1}{2}\left\{\mathrm{Re}\left[F(k)\right] + \mathrm{Re}\left[F(M-k)\right]\right\} + \frac{j}{2}\left\{\mathrm{Im}\left[F(k)\right] - \mathrm{Im}\left[F(M-k)\right]\right\} \quad (8)$$

and

$$X_2(k) = \frac{1}{2}\left\{\mathrm{Im}\left[F(k)\right] + \mathrm{Im}\left[F(M-k)\right]\right\} + \frac{j}{2}\left\{\mathrm{Re}\left[F(M-k)\right] - \mathrm{Re}\left[F(k)\right]\right\} \quad (9)$$

where M is the number of the FFT points and $F(k)$ is the Fourier transform of the complex signal

$$f(n) = x_1(n) + jx_2(n). \quad (10)$$

We refer to the execution of (8) and (9) as FFT decomposition.

With the above considerations, a schematic diagram of DSPP signal flow is shown in Fig. 2. The scale factor $2^{b_1}/C_l$ is chosen such that overflow probability is small during A/D conversion where b_1 is the number of the bits of the A/D excluding the sign bit and C_l is the clipping level of the A/D. The output of the A/D is left-shifted b bits to become the input of the FFT. Let b_2 be the number of bits of FFT. Then $b_1 + b$ must be no more than b_2 to prevent overflow in the input of the FFT. As previously mentioned, a scale factor $1/M$ will be used within the FFT for preventing FFT overflow. The scale factors 2^{d_1} and 2^{d_2} are used for simplifying the complexity of the FFT

decomposition and the window weight setting. The l least significant bits of the periodogram are dropped prior to the final triple summation in order to minimize the number of bits in the output of the triple summation. Only a fixed number of bits of the output of the triple summation are kept by dropping "a" bits. Of course, all the scale factors must be compensated for when computing $\hat{P}_R$. Note that the compensation factor

$$A = C_l^2 2^{l-2b_1-2b-2d_1-2d_2} \tag{11}$$

is used in the computation of $\hat{P}_R$ (see Fig. 2).

In this paper, we assume that the dynamic range in each stage is large enough such that the overflow is negligible. Fixed-point arithmetic is assumed.

III. Roundoff Noise Modeling Assumptions

Quantization errors occur when an analog signal is converted to a digital representation with a fixed word length. Errors will also be generated during arithmetic operations on finite-length digital numbers. Right bit-shifting operations, which are equivalent to truncation, can also result in errors. We have called all these errors roundoff noise. For fixed-point arithmetic, only multiplication of two digital numbers and truncation of the least significant bits produce errors. The roundoff noise due to multiplication operation can be eliminated at the expense of increasing the word length after multiplication.

In this paper we assume the signal path from the A/D input to the output of the triple summation is implemented by a special-purpose digital processor. In NSCAT, this processor will be on board a spacecraft. The roundoff noise generated in this processor must be accounted for in the design when determining processor performance. However, roundoff noise generated in the signal processing after the triple summation is assumed negligible. For NSCAT, this processing will be performed on ground.

In Fig. 3, we show the roundoff noise sources occurring in the model shown in Fig. 2. e_1 and e_1' are generated by the A/D conversion. No error is generated by the scale factor 2^b (left bit-shift by b bits). e_2 and e_2' are generated by the FFT computation. e_3 and e_3' are generated by the decomposition of the FFT output. e_4 and e_4' are generated by windowing. e_5 and e_5' are generated by the squaring operation. e_6 is generated by the presummation scale factor (truncation of l least significant bits). e_7 is generated by the postsummation scale factor (truncation of "a" least significant bits). Notice that e_2 and e_2', generated during FFT computation, and e_4 and e_4', generated in performing convolution, consist of many arithmetic steps.

In Fig. 3, we denote the actual digital signal at each stage by $y_i(k)$ or $y_i'(k)$. Let $f_i(k)$ and $f_i'(k)$ denote the ideal digital signals associated with $y_i(k)$ and $y_i'(k)$, respectively. The resulting roundoff noise, $h_i(k)$ or $h_i'(k)$, propagated from the previous stages, is then

$$h_i(k) = y_i(k) - f_i(k) \tag{12a}$$

or

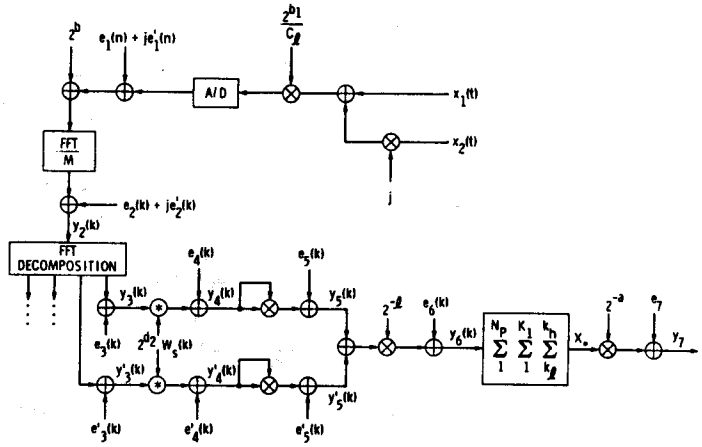

Fig. 3. Roundoff error sources in the DSPP shown in Fig. 2. In the triple summation, $N_P = N_{PS}$, $K_1 = K_S$, $k_h = k_{HS}$, and $k_l = k_{LS}$ for the signal-plus-noise case; $N_P = N_{PN}$, $K_1 = K_N$, $k_h = k_{HN}$, and $k_l = k_{LN}$ for the noise-only case.

$$h_i'(k) = y_i'(k) - f_i'(k). \tag{12b}$$

We can easily eliminate some noise sources by the appropriate choice of scale factors. We make $e_3 = e_3' = 0$ by choosing $d_1 = 1$ [see (8) and (9)]. We can make $e_5 = e_5' = 0$ by increasing the word length of the output of the squaring operation.

We now make the following assumptions about all the roundoff noises.

(A3) $e_3 = 0$, $e_3' = 0$, $e_5 = 0$, and $e_5' = 0$.

(A4) All the noise sources are independent of one another and are independent of the signal.

(A5) The accumulated roundoff noises $h_4(k)$ and $h_4'(k)$ at the input to the squaring operation are Gaussian.

Assumption (A4) is generally used in the roundoff noise analysis of digital signal processors. Assumption (A5) is made to simplify the following derivation. From Fig. 3, one can easily see that all signal processing procedures are linear except for the squaring operation. The derivation of second-order statistics of the output of the squaring block requires fourth-order statistics of its input. This will make the derivation extremely difficult without the last assumption. We also note that by the central-limit theorem, the last assumption is reasonable.

IV. Roundoff Noise-to-Signal Ratio V

From Fig. 3, we can see that the signal processing procedure from the input to $y_4(k)$ or $y_4(k)'$ is linear and that the signal processing procedure after $y_5(k)$ or $y_5(k)'$ is also linear. The only nonlinear operation is the square which makes the roundoff noise $h_5(k)$ accumulated in $y_5(k)$ correlated to the true signal. Therefore, $h_5(k)$ is correlated between different data segments because the true signals in $y_5(k)$ are correlated with one another due to the time overlapping processing of the input signal. So is $h_5'(k)$. For notational simplicity, we neglect the indexes associated with the data segment number for the signal path from the input through $y_4(k)$. From $y_5(k)$ on we will attach the data segment number to all the quantities by a superscript (i).

The derivation for the roundoff noise-to-signal ratio consists of the following 5-step procedure:

Step A: mean and covariance function of $h_4(k)$ and $h_4'(k)$;
Step B: mean and covariance function of $h_5(k)$ and $h_5'(k)$;
Step C: mean and variance of h_7;
Step D: mean and variance of roundoff noise in $\hat{P}_R$; and
Step E: roundoff noise-to-signal ratio V.

This 5-step derivation procedure provides a set of equations. These equations have to be sequentially computed to obtain V. In each step we present the derivations and results as concisely as possible with detailed proofs shown in Appendix A. The following derivation is for the signal-plus-noise case. Results for the noise-only case can be similarly obtained. We use m_i and σ_i^2 to denote the mean and variance of e_i, respectively. Note that e_i and e_i' have the same mean and variance. Let $\phi_i(k)$ and $\phi_i'(k)$ be the covariance function of $h_i(k)$ and $h_i'(k)$, respectively.

Step A: Mean and covariance function of $h_4(k)$ and $h_4'(k)$.

From Fig. 3,

$$h_2(k) = \frac{2^b}{M} \sum_{n=0}^{M-1} \left(e_1(n) + je_1'(n)\right) \exp\left\{-j2\pi nk/M\right\} + \left(e_2(n) + je_2'(n)\right). \tag{13}$$

Based on our assumptions, it can be easily shown that

$$E\left\{\text{Re}\left[h_2(k)\right]\right\} = E\left\{\text{Im}\left[h_2(k)\right]\right\} = 2^b m_1 \delta(k) + m_2 \tag{14}$$

where $\delta(k)$ is the unit sample sequence, and that Re $[h_2(k)]$ and Im $[h_2(k)]$ are uncorrelated with each other and both are white processes with variance $\sigma^2/2$ where

$$\sigma^2 = \text{Var}\left[h_2(k)\right] = \frac{2^{2b+1}}{M}\sigma_1^2 + 2\sigma_2^2. \tag{15}$$

Because

$$h_3(k) = \text{Re}\left[h_2(k)\right] + \text{Re}\left[h_2(M-k)\right] \tag{16a}$$

$$h_3'(k) = \text{Im}\left[h_2(k)\right] - \text{Im}\left[h_2(M-k)\right] \tag{16b}$$

for $0 \le k \le M-1$, one can easily show that

$$E[h_3(k)] = E\left\{\text{Re}\left[h_2(k)\right] + \text{Re}\left[h_2(M-k)\right]\right\} = 2E\left\{\text{Re}\left[h_2(k)\right]\right\}, \tag{17a}$$

$$E[h_3'(k)] = 0, \tag{17b}$$

and

$$\phi_3(k) = \phi_3'(k) = \sigma^2\delta(k). \tag{18}$$

Note, from (16a) and (16b), that $h_3(k)$ is uncorrelated with $h_3'(k)$ although they have the same covariance function.

The windowing output $h_4(k)$ is

$$h_4(k) = h_3(k) * 2^{d_2}W_S(k) = \frac{2^{d_2}}{M}\sum_{n=0}^{M-1} h_3(n)\, W_S(k-n) + e_4(k). \tag{19}$$

From (14), (17a), (18), and (19),

$$E[h_4(k)] = 2^{d_2+1}m_2 w_S(0) + (2^{b+1}m_1) \cdot \left(\frac{2^{d_2}}{M}W_S(k)\right) + m_4 \tag{20}$$

and

$$\phi_4(k) = \sigma^2\phi_W(k) + \sigma_4^2 \tag{21}$$

where

$$\phi_W(k) = \frac{2^{2d_2}}{M^2}\sum_{n=0}^{M-1} W_S(n)\, W_S(n+k). \tag{22}$$

Similarly, one can show that

$$E[h_4'(k)] = m_4, \tag{23}$$

and

$$\phi_4'(k) = \phi_4(k). \tag{24}$$

Note, from (20) and (23), that $E[h_4(k)]$ is a function of k but $E[h_4'(k)]$ is not. Also note that $h_4(k)$ is uncorrelated with $h_4'(k)$ although they have the same covariance function.

Step B: Mean and covariance function of $h_5^{(i)}(k)$ and $h_5'^{(i)}(k)$.

Note that

$$h_5^{(i)}(k) = y_5^{(i)}(k) - f_5^{(i)}(k) = \left[f_4^{(i)}(k) + h_4^{(i)}(k)\right]^2 - \left(f_4^{(i)}(k)\right)^2 = \left(h_4^{(i)}(k)\right)^2 + 2h_4^{(i)}(k)\, f_4^{(i)}(k). \tag{25}$$

Since $E[f_4^{(i)}(k)] = 0$ (see [1]), then

$$E\left[h_5^{(i)}(k)\right] = E\left[h_4^2(k)\right] = \phi_4(0) + E^2\left[h_4(k)\right]. \tag{26}$$

Note that the superscript (i) associated with $h_4(k)$ is omitted because its mean and covariance are independent of data segment index i. Similarly, we have

$$h_5'^{(r)}(k) = \left(h_4'^{(r)}(k)\right)^2 + 2h_4'^{(r)}(k)\, f_4'^{(r)}(k) \tag{27}$$

and

$$E\left[h_5'^{(r)}(k)\right] = E\left[h_4'^2(k)\right] = \phi_4'(0) + E^2\left[h_4'(k)\right]. \tag{28}$$

Next, we derive the covariances Cov $\{h_5^{(i)}(k_1), h_5^{(r)}(k_2)\}$, Cov $\{h_5'^{(i)}(k_1), h_5'^{(r)}(k_2)\}$, and Cov $\{h_5^{(i)}(k_1), h_5'^{(r)}(k_2)\}$.

One can easily see that

$$\text{Cov}\left\{h_4^{(i)}(k_1), h_4^{(r)}(k_2)\right\} = 0, \quad i \ne r, \tag{29}$$

because they are associated with the different data segments which are processed separately. Similarly, one can see that

$$\text{Cov}\left\{h_4'^{(i)}(k_1), h_4'^{(r)}(k_2)\right\} = 0, \quad i \neq r. \tag{30}$$

As concluded in the derivation of step A, we have

$$\text{Cov}\left\{h_4^{(i)}(k_1), h_4'^{(r)}(k_2)\right\} = 0. \tag{31}$$

Equations (29)–(31) imply the following results.

(R1) $h_4^{(i)}(k_1)$ is independent of $h_4^{(r)}(k_2)$ for $i \neq r$.

(R2) $h_4'^{(i)}(k_1)$ is independent of $h_4'^{(r)}(k_2)$ for $i \neq r$.

(R3) $h_4^{(i)}(k_1)$ is independent of $h_4'^{(r)}(k_2)$.

These results are obtained because $h_4^{(i)}(k)$ and $h_4'^{(i)}(k)$ are assumed to be Gaussian in assumption (A5). Based on assumption (A4) and the fact that $E[f_4^{(i)}(k)] = E[f_4'^{(i)}(k)] = 0$, one can easily show that

$$\text{Cov}\left\{\left(h_4^{(i)}(k_1)\right)^2, h_4^{(r)}(k_2) f_4^{(r)}(k_2)\right\} = 0, \tag{32}$$

$$\text{Cov}\left\{\left(h_4'^{(i)}(k_1)\right)^2, h_4'^{(r)}(k_2) f_4'^{(r)}(k_2)\right\} = 0, \tag{33}$$

$$\text{Cov}\left\{\left(h_4^{(i)}(k_1)\right)^2, h_4'^{(r)}(k_2) f_4'^{(r)}(k_2)\right\} = 0, \tag{34}$$

and

$$\text{Cov}\left\{\left(h_4'^{(i)}(k_1)\right)^2, h_4^{(r)}(k_2) f_4^{(r)}(k_2)\right\} = 0. \tag{35}$$

The covariances associated with $f_4^{(i)}(k)$ and $f_4'^{(i)}(k)$ are given by

$$\begin{aligned} G_{ir}(k_1, k_2) &= E[f_4^{(i)}(k_1) f_4^{(r)}(k_2)] \\ &= E[f_4'^{(i)}(k_1) f_4'^{(r)}(k_2)] \end{aligned} \tag{36}$$

and

$$G'_{ir}(k_1, k_2) = E[f_4^{(i)}(k_1) f_4'^{(r)}(k_2)]. \tag{37}$$

These results are derived in Appendix A. We note that

$$\begin{aligned} G_{ii}(k_1, k_2) &= G_{ii}(k_2, k_1) = \phi_f^{(i)}(k_1 - k_2) \\ &= \phi_f'^{(i)}(k_1 - k_2) \end{aligned} \tag{38}$$

where $\phi_f^{(i)}(k)$ and $\phi_f'^{(i)}(k)$ are the autocovariance functions of $f_4^{(i)}(k)$ and $f_4'^{(i)}(k)$, respectively. From (25), (27), (32)–(37) and the results (R1), (R2), and (R3) one can easily show that

$$\text{Cov}\left\{h_5^{(i)}(k_1), h_5^{(r)}(k_2)\right\} = 4E[h_4^{(i)}(k_1)]\, E[h_4^{(r)}(k_2)]\, G_{ir}(k_1, k_2), \quad i \neq r, \tag{39}$$

$$\text{Cov}\left\{h_5'^{(i)}(k_1), h_5'^{(r)}(k_2)\right\} = 4E[h_4'^{(i)}(k_1)]\, E[h_4'^{(r)}(k_2)]\, G_{ir}(k_1, k_2), \quad i \neq r, \tag{40}$$

$$\text{Cov}\left\{h_5^{(i)}(k_1), h_5'^{(r)}(k_2)\right\} = 4E[h_4^{(i)}(k_1)]\, E[h_4'^{(r)}(k_2)]\, G'_{ir}(k_1, k_2), \tag{41}$$

and

$$\text{Cov}\left\{h_5'^{(i)}(k_1), h_5^{(r)}(k_2)\right\} = 4E[h_4'^{(i)}(k_1)]\, E[h_4^{(r)}(k_2)]\, G'_{ri}(k_2, k_1). \tag{42}$$

Next, we derive Cov $\{h_5^{(i)}(k_1), h_5^{(i)}(k_2)\}$ and Cov $\{h_5'^{(i)}(k_1), h_5'^{(i)}(k_2)\}$.

Using the well-known equation for the covariance of x^2 and y^2 where x and y are two joint Gaussian random variables [9]

$$\begin{aligned} \text{Cov}\{x^2, y^2\} &= 2[\text{Cov}\{x, y\}]^2 \\ &\quad + 4\,\text{Cov}\{x, y\}\, E[x]\, E[y] \end{aligned} \tag{43}$$

and based on the assumption (A5), we obtain

$$\begin{aligned} &\text{Cov}\left\{h_4^2(k_1), h_4^2(k_2)\right\} \\ &= 2\phi_4^2(k_1 - k_2) + 4E[h_4(k_1)]\, E[h_4(k_2)]\, \phi_4(k_1 - k_2). \end{aligned} \tag{44}$$

Therefore, from (25), (32), and (44) we obtain

$$\begin{aligned} \text{Cov}\left\{h_5^{(i)}(k_1), h_5^{(i)}(k_2)\right\} &= \text{Cov}\left\{h_4^2(k_1), h_4^2(k_2)\right\} \\ &\quad + 4E[h_4(k_1)\, h_4(k_2)]\, E[f_4^{(i)}(k_1) f_4^{(i)}(k_2)] \\ &= 2\phi_4^2(k_1 - k_2) + 4E[h_4(k_1)]\, E[h_4(k_2)] \\ &\quad (\phi_4(k_1 - k_2) + \phi_f^{(i)}(k_1 - k_2)) \\ &\quad + 4\phi_4(k_1 - k_2)\, \phi_f^{(i)}(k_1 - k_2). \end{aligned} \tag{45}$$

Similarly, we have

$$\begin{aligned} &\text{Cov}\left\{h_5'^{(i)}(k_1), h_5'^{(i)}(k_2)\right\} \\ &= 2\phi_4'^2(k_1 - k_2) + 4E[h_4'(k_1)]\, E[h_4'(k_2)] \\ &\quad \cdot (\phi_4'(k_1 - k_2) + \phi_f'^{(i)}(k_1 - k_2)) \\ &\quad + 4\phi_4'(k_1 - k_2)\, \phi_f'^{(i)}(k_1 - k_2). \end{aligned} \tag{46}$$

Step C: Mean and variance of h_7.

From Fig. 3, one can see that

$$h_6^{(i)}(k) = 2^{-l}\left(h_5^{(i)}(k) + h_5'^{(i)}(k)\right) + e_6^{(i)}(k). \tag{47}$$

Thus,

$$E[h_6^{(i)}] = 2^{-l}\left(E[h_5^{(i)}(k)] + E[h_5'^{(i)}(k)]\right) + m_6 \tag{48}$$

and

$$\begin{aligned} &\text{Cov}\left\{h_6^{(i)}(k_1), h_6^{(r)}(k_2)\right\} \\ &= 2^{-2l}[\text{Cov}\left\{h_5^{(i)}(k_1), h_5^{(r)}(k_2)\right\} \\ &\quad + \text{Cov}\left\{h_5^{(i)}(k_1), h_5'^{(r)}(k_2)\right\} \\ &\quad + \text{Cov}\left\{h_5'^{(i)}(k_1), h_5^{(r)}(k_2)\right\} \\ &\quad + \text{Cov}\left\{h_5'^{(i)}(k_1), h_5'^{(r)}(k_2)\right\}] \\ &\quad + \sigma_6^2 \delta(k_1 - k_2)\, \delta(i - r). \end{aligned} \tag{49}$$

Let

$$h_7^* = \sum_{i=1}^{K_S} \sum_{k=k_{LS}}^{k_{HS}} h_6^{(i)}(k). \tag{50}$$

Then

$$E[h_7^*] = \sum_{i=1}^{K_S} \sum_{k=k_{LS}}^{k_{HS}} E\left[h_6^{(i)}(k)\right] \tag{51}$$

and

$$\text{Var}\,[h_7^*] = \sum_{i=1}^{K_S} \sum_{r=1}^{K_S} \sum_{k_1=k_{LS}}^{k_{HS}} \sum_{k_2=k_{LS}}^{k_{HS}} \text{Cov}\left\{h_6^{(i)}(k_1), h_6^{(r)}(k_2)\right\}. \tag{52}$$

Finally, h_7 is the sum of h_7^*'s associated with N_{PS} independent pulses multiplied by 2^{-a}. Thus,

$$E[h_7] = 2^{-a} N_{PS} E[h_7^*] + m_7 \tag{53}$$

and

$$\text{Var}\,[h_7] = 2^{-2a} N_{PS}\left\{\text{Var}\,[h_7^*]\right\} + \sigma_7^2. \tag{54}$$

As a remark, from (25) and (27), one can easily show that $h_5^{(i)}(k)$ is uncorrelated with the true signal $(f_4^{(i)}(k))^2$ and $h_5'^{(i)}(k)$ is uncorrelated with the true signal $(f_4'^{(i)}(k))^2$. Because h_7 is a linear function of $h_5^{(i)}(k)$ and $h_5'^{(i)}(k)$, and the true signal f_7 is a linear function of $(f_4^{(i)}(k))^2$ and $(f_4'^{(i)}(k))^2$, h_7 is uncorrelated with f_7.

Step D: Mean and variance of roundoff noise in $\hat{P}_R$.

Let $\epsilon_{SN} = h_7$ for signal-plus-noise case and $\epsilon_N = h_7$ for the noise-only case. Then the roundoff noise ϵ, embedded in $\hat{P}_R$, is given by

$$\epsilon = \frac{U_S T}{U_S^* T_{GS}}\left(\frac{AM2^{a_S}}{U_S K_S N_{PS}}\epsilon_{SN} - \frac{AN2^{a_N}}{U_N K_N N_{PN}}\frac{T_{GS}B_S}{T_{GN}B_N}\epsilon_N\right) \tag{55}$$

where a_S and a_N are the values of "a" associated with ϵ_{SN} and ϵ_N, respectively. Therefore,

$$E[\epsilon] = \frac{U_S T}{U_S^* T_{GS}}\left(\frac{AM2^{a_S}}{U_S K_S N_{PS}} E[\epsilon_{SN}] - \frac{AN2^{a_N}}{U_N K_N N_{PN}}\frac{T_{GS}B_S}{T_{GN}B_N} E[\epsilon_N]\right) \tag{56}$$

and

$$\text{Var}\,[\epsilon] = \left(\frac{U_S T}{U_S^* T_{GS}}\right)^2\left\{\left(\frac{AM2^{a_S}}{U_S K_S N_{PS}}\right)^2 \text{Var}\,[\epsilon_{SN}] + \left(\frac{AN2^{a_N}}{U_N K_N N_{PN}}\right)^2\left(\frac{T_{GS}B_S}{T_{GN}B_N}\right)^2 \text{Var}\,[\epsilon_N]\right\}. \tag{57}$$

Step E: Roundoff noise-to-signal ratio V.

Let $\hat{P}_R'$ be the actual measurement of P_R, i.e.,

$$\hat{P}_R' = \hat{P}_R + \epsilon. \tag{58}$$

We define the roundoff noise-to-signal ratio V as

$$V = \left(\frac{E[\epsilon^2]}{E[\hat{P}_R^2]}\right)^{1/2}. \tag{59}$$

Since $\hat{P}_R$ is an unbiased estimate of P_R with mean square value

$$E[\hat{P}_R^2] = (1 + K_p^2) P_R^2, \tag{60}$$

substituting (60) into (59) gives

$$V = \frac{K_{pe}}{(1 + K_p^2)^{1/2}} \tag{61}$$

where

$$K_{pe} = \frac{1}{P_R}\left\{E[\epsilon^2]\right\}^{1/2} = \frac{1}{P_R}\left(\text{Var}[\epsilon] + E^2[\epsilon]\right)^{1/2}. \tag{62}$$

K_{pe} can be thought of as the normalized root mean square value due to the effects of roundoff noise.

V. A Design Example

In this section, we illustrate the computation of roundoff noise-to-signal ratio V and compare the theoretical results to simulation results using an example associated with the design of the DDP in NSCAT.

Practical considerations and performance requirements dictate the following choice of parameters for the NSCAT DDP design:

$$b_2 = 16 \text{ (bits in FFT)},$$
$$d_1 = 1,$$
$$d_2 = 2,$$
$$M = N = 512,$$
$$D = M/2 \text{ (i.e., 50 percent overlap)},$$
$$2 \le k_{LS} \le k_{HS} \le M/2 - 1$$

and $w_S(n) = w_N(n)$ is a Hanning window, i.e.,

$$w_S(n) = 0.5 - 0.5\cos\left(\frac{2\pi n}{M}\right), \quad 0 \le n \le M - 1. \tag{63}$$

$W_S(k)$ is then

$$W_S(k) = \begin{cases} \dfrac{M}{2}, & k = 0; \\ -\dfrac{M}{4}, & k = 1, M-1; \\ 0, & \text{otherwise.} \end{cases} \tag{64}$$

For this case, $e_4(k) = 0$ because no multiplications are needed during windowing. Only left bit-shifting and addition are performed. For this example, some intermediate equations in the previous section can be simplified. In Appendix B, we list these intermediate equations and briefly discuss the m_i and σ_i^2 to be used in computing the roundoff noise-to-signal ratio V.

Let X_* be the output signal of the triple summation block before truncating "a" bits in Fig. 3. The dynamic range of X_* for the signal-plus-noise case is much larger than that for the noise-only case. Therefore, it is judicious to make "a" adaptive. The following approach for determing a is assumed.

Let q be the number of bits of X_*, i.e.,

$$q = [\log_2 X_*]^+ \tag{65}$$

where $[x]^+$ denotes the smallest integer larger than x. The value a is determined as follows:

$$a(q) = \begin{cases} q - n_{\max}, & \text{if } q - n_{\max} \geq a_{\min}; \\ a_{\min}, & \text{otherwise,} \end{cases} \tag{66}$$

where $n_{\max}$ is the maximum number of bits for y_7 after "a" bits truncation, and $a_{\min}$ is the minimum value of "a." Note that "a" is a function of q. Let

$$q_* = [\log_2 E[X_*]]^+. \tag{67}$$

One can also show that $\mathrm{Var}^{1/2}[X_*]/E[X_*] \ll 1/2$, which implies q will take the value q_* with very high probability. The value "a" for the theoretical calculation is chosen to be the value for $q = q_*$ in (66).

We performed computer simulations for this example to validate the theoretical results derived in the previous section. The realization of the DDP in Fig. 2 with finite word length was simulated by a digital computer. The ideal DDP with infinite word length cannot be simulated with a finite-word-length digital computer. Therefore, the "pseudoideal" DDP was simulated by a digital computer with floating-point arithmetic. Of course, all the digital numbers in the "pseudoideal" DDP have many more bits than in the realization of the DDP with finite word length. We then generated a set of Gaussian random sequences as input to the simulated DDP to get $\hat{P}_R'$ as well as to input to a "pseudoideal" DDP to get $\hat{P}_R$. We then computed the statistical mean square value of the roundoff error $\epsilon = \hat{P}_R' - \hat{P}_R$, and then use (61) and (62) to calculate the roundoff noise-to-signal ratio V. In the following simulations, $k_N = k_S = 32$, $N_{PN} = 4$, and $n_{\max} = 12$. Only the parameters b, b_1, N_{PS}, l, and $a_{\min}$ were varied.

Table II shows the analytical and simulated results for three cases with $l = 2$, $a_{\min} = 6$. In the first case, shown in Table II(a), we used the parameters $N_{PS} = 25$, $b_1 = 7$, and $b = 7$; and the second case, shown in Table II(b), we used $N_{PS} = 4$, $b_1 = 5$, and $b = 9$. For the third case, shown in Table II(c), we used $N_{PS} = 4$, $b_1 = 7$, and $b = 7$. From Table II, we can see that our predicted results agree well with our simulation results. Note that V is larger for smaller SNR for all three cases. The results in Table II(a) are very similar to those in Table II(c). This implies that roundoff noise-to-signal ratio is not sensitive to N_{PS}. The insensitivity to N_{PS} can also be directly predicted by (54), (57), (61), (62), and (7) by noting that the numerator and the denominator of (54) have the same order of N_{PS}. On the other hand, the results in Table II(b), which are much larger than those in Table II(c), imply that roundoff noise-to-signal ratio is very sensitive to the number of A/D bits. Note, from Table II(b) and (c), that the roundoff noise-to-signal ratio reduction is about 6 dB for a 2 bit increase in the A/D conversion. In other words, the roundoff noise-to-signal ratio reduction is about 3 dB per A/D bit. This will be considered further below.

TABLE II
ANALYTICAL RESULTS AND SIMULATED RESULTS FOR $l = 2$, $a_{\min} = 6$, AND (a) $N_{PS} = 25$, $b_1 = b = 7$; (b) $N_{PS} = 4$, $b_1 = 5$, $b = 9$; (c) $N_{PS} = 4$, $b_1 = b = 7$

	Roundoff noise-to-signal ratio V (percent)					
SNR (db)	@@	**	@@	**	@@	**
-20	8.04	7.43	28.8	30.4	8.04	7.69
-15	7.66	7.00	27.9	30.2	7.78	7.36
-10	5.57	5.13	22.5	22.1	6.27	5.98
-5	2.37	2.15	11.2	10.8	3.12	2.95
0	0.82	0.75	4.34	4.42	1.21	1.17
5	0.29	0.27	1.82	1.82	0.51	0.47
10	0.12	0.12	0.88	0.88	0.25	0.23
15	0.06	0.07	0.46	0.46	0.13	0.13
	(a)		(b)		(c)	

@@ Analytical results ** Simulation results

We have observed that the reduction of roundoff noise-to-signal is about 3 dB per A/D bit in Table II(b) and (c). We now consider additional analytical predictions for this case. The roundoff noise-to-signal ratios for $b_1 = 4, 5, 6, 7, 8$, and 9 are shown in Table IV. The 3 dB per A/D bit in the reduction of roundoff noise-to-signal ratio can be seen for the values of b_1 between 4–6. However, the reduction in the roundoff noise-to-signal ratio is different for cases $b_1 = 6$, through 9. While the reduction in the roundoff noise-to-signal ratio between $b_1 = 6$ and $b_1 = 7$ is about 2.6 dB, the reduction in the roundoff noise-to-signal ratio between $b_1 = 7$ and $b_1 = 8$ is about 1.9 dB. The reduction in the roundoff noise-to-signal ratio between $b_1 = 8$ and $b_1 = 9$ is only 0.9 dB. The amount of the reduction in V per bit decreases as the number of the A/D bits (b_1) increases. The roundoff noise generated by the A/D conversion dominates V for small b_1. As the number of A/D bits increases, the A/D noise decreases until it no longer dominates V.

For the set of cases shown in Table III we used $N_{PS} = 4$, $b_1 = b = 7$. We show the analytical results for various values of l and $a_{\min}$. From this table, it is observed that the effects of roundoff noise are the same for constant $l + a_{\min}$. We can see that V increases as l increases. This follows intuition.

TABLE III
ANALYTICAL RESULTS FOR $N_{PS} = 4$, $b_1 = b = 7$, AND VARIOUS VALUES OF l AND a_{min}

Roundoff noise-to-signal ratio V (percent)

		SNR (db)							
a_{min}	l	-20	-15	-10	-5	0	5	10	15
6	2	8.04	7.78	6.27	3.12	1.21	0.51	0.25	0.13
4	4	8.04	7.78	6.27	3.12	1.21	0.51	0.25	0.13
2	6	8.04	7.78	6.27	3.12	1.21	0.51	0.25	0.13
0	8	8.04	7.78	6.27	3.12	1.21	0.51	0.25	0.13
0	10	8.04	7.83	6.31	3.14	1.22	0.51	0.25	0.13
0	12	8.73	8.45	6.79	3.36	1.28	0.53	0.25	0.13
0	14	15.8	15.3	12.2	5.84	2.08	0.74	0.30	0.14

TABLE IV
ANALYTICAL RESULTS FOR $l = 2$, $a_{min} = 6$, $N_{PS} = 4$, $b = 14 - b_1$, AND VARIOUS VALUES OF b_1

Roundoff noise-to-signal ratio V (percent)

SNR	b_1					
(db)	4	5	6	7	8	9
-20	58.99	28.82	14.68	8.041	5.207	4.212
-15	57.09	27.90	14.21	7.784	5.041	4.078
-10	45.94	22.47	11.45	6.272	4.062	3.286
-5	22.79	11.18	5.699	3.122	2.022	1.636
0	8.793	4.337	2.215	1.214	0.787	0.636
5	3.650	1.816	0.929	0.510	0.331	0.268
10	1.748	0.876	0.449	0.248	0.162	0.132
15	0.922	0.463	0.238	0.132	0.087	0.071

VI. DISCUSSION AND CONCLUSIONS

In this paper, we have presented a roundoff noise analysis for DSPP's using Welch's power spectrum estimation based on reasonable assumptions for the signal and quantization error models. Overflow is assumed to be negligible in our analysis. Instead of providing an extremely complicated equation for computing the roundoff noise-to-signal ratio V in the measurement of signal power P_R, we have derived a set of equations that can be used to compute V.

As mentioned in Section II, the practical implementation of a digital signal processor is driven not only by the roundoff noise level but also by the dynamic range at each stage of processing. The digital processor may incur some untractable nonlinear effect if overflow occurs. One can compute the mean and variance of the signal at each stage to compute the probability of occurrence of overflow. Then one can also determine the dynamic range needed in each stage to make this probability small. To prevent overflow, many bits at each stage of processing are preferred. Since the number of bits at each stage determines hardware complexity, discarding some least significant bits would make the hardware implementation more feasible. However, the value of V depends on the number of bits used in each stage. By computing V for a hardware design, one can observe if the performance of this design is satisfactory. From the simulation example presented in Section V which supports our analytical results, one can see that V is more sensitive to certain parameters than others and that V may be the same for some combinations of parameters. The derived results have been used to minimize the hardware complexity of the DDP for NSCAT, which we will report in a separate paper.

Fixed-point arithmetic is assumed in this paper. The results for the floating-point arithmetic can be similarly obtained. We believe that the roundoff analysis presented in this paper will be helpful in designing other digital signal processors for estimating signal power.

APPENDIX A
COVARIANCES ASSOCIATED WITH $f_4^{(i)}(k)$ AND $f_4'^{(i)}(k)$

In this appendix, we show that

$$G_{ir}(k_1, k_2) = E[f_4^{(i)}(k_1) f_4^{(r)}(k_2)] = E[f_4'^{(i)}(k_1) f_4^{(r)}(k_2)] \quad \text{(A1)}$$

and

$$G'_{ir}(k_1, k_2) = E[f_4^{(i)}(k_1) f_4'^{(r)}(k_2)] \quad \text{(A2)}$$

where $G_{ir}(k_1, k_2)$ and $G'_{ir}(k_1, k_2)$ are defined as follows.

1) Signal-Plus-Noise Case:

$$G_{ir}(k_1, k_2) = \left(\frac{2^{b_1+b+d_1+d_2}}{MC_l}\right)^2 \left(\frac{P_R}{2B_S T}\right) \text{Re}\,[L_{ir}(k_1, k_2)], \quad \text{(A3)}$$

$$G'_{ir}(k_1, k_2) = -\left(\frac{2^{b_1+b+d_1+d_2}}{MC_l}\right)^2 \left(\frac{P_R}{2B_S T}\right) \text{Im}\,[L_{ir}(k_1, k_2)] \quad \text{(A4)}$$

where

$$L_{ir}(k_1, k_2) = \left[\Gamma_{ir}(k_1 - k_2) + \frac{1}{\text{SNR}} W_S(i - r, k_1 - k_2)\right] \cdot \exp\{j2\pi k_2 (i - r) D/M\}. \quad \text{(A5)}$$

2) Noise-Only Case:

$$G_{ir}(k_1, k_2) = \left(\frac{2^{b_1+b+d_1+d_2}}{NC_l}\right)^2 \left(\frac{b'}{2T}\right) \cdot \text{Re}\,[W_N(i - r, k_1 - k_2) \cdot \exp\{j2\pi k_2 (i - r) D/N\}], \quad \text{(A6)}$$

$$G'_{ir}(k_1, k_2) = -\left(\frac{2^{b_1+b+d_1+d_2}}{NC_l}\right)^2 \left(\frac{b'}{2T}\right) \cdot \text{Im}\,[W_N(i - r, k_1 - k_2) \cdot \exp\{j2\pi k_2 (i - r) D/N\}]. \quad \text{(A7)}$$

Proof:

Case I: Signal-Plus-Noise Case: In [1], we express

$$f_4^{(i)}(\omega) = \frac{2^{b_1+b+d_1+d_2}}{MC_l} \operatorname{Re}\left[X_{si}(\omega) + X_{ni}(\omega)\right] \quad \text{(A8)}$$

and

$$f_4'^{(i)}(\omega) = \frac{2^{b_1+b+d_1+d_2}}{MC_l} \operatorname{Im}\left[X_{si}(\omega) + X_{ni}(\omega)\right] \quad \text{(A9)}$$

where $X_{si}(\omega)$ and $X_{ni}(\omega)$ are the Fourier transforms of $s_i(m)\ \gamma_i(m)$ and $n_i(m)\ w_S(m)$, respectively, and $s_i(m)$ and $n_i(m)$ are defined as

$$n_i(m) = n(m + (i-1)D) \quad \text{(A10)}$$

and

$$s_i(m) = s(m + (i-1)D). \quad \text{(A11)}$$

Note that $s(m)$ is the true input signal.

Let

$$I_i(\omega) = 2 \operatorname{Re}\left[X_{si}(\omega) + X_{ni}(\omega)\right] = \left[X_{si}(\omega) + X_{si}^*(\omega)\right] + \left[X_{ni}(\omega) + X_{ni}^*(\omega)\right]. \quad \text{(A12)}$$

Then, from [1] we have

$$\begin{aligned}&\operatorname{Cov}\left\{I_i(\omega_1), I_r(\omega_2)\right\}\\ &= 2E\Big\{\operatorname{Re}\left[X_{si}(\omega_1)\, X_{sr}(\omega_2) + X_{si}(\omega_1)\, X_{sr}^*(\omega_2)\right]\\ &\quad + \operatorname{Re}\left[X_{ni}(\omega_1)\ X_{nr}(\omega_2) + X_{ni}(\omega_1)\, X_{nr}^*(\omega_2)\right]\Big\}\\ &\approx \frac{2P_R}{B_S T} \operatorname{Re}\left\{\Gamma_{ir}(\omega_1 - \omega_2) \exp\left\{j\omega_2(i-r)D\right\}\right\}\\ &\quad + \frac{2b'}{T} \operatorname{Re}\left\{W_S(i-r, \omega_1 - \omega_2) \exp\left\{j\omega_2(i-r)D\right\}\right\}\\ &= \frac{2P_R}{B_S T} \operatorname{Re}\left\{L_{ir}(\omega_1, \omega_2)\right\}. \end{aligned} \quad \text{(A13)}$$

Therefore, from (A8), (A12), and (A13), we have

$$E\left[f_4^{(i)}(k_1)\, f_4^{(r)}(k_2)\right] = G_{ir}(k_1, k_2). \quad \text{(A14)}$$

Let

$$\begin{aligned}J_i(\omega) &= 2 \operatorname{Im}\left[X_{si}(\omega) + X_{ni}(\omega)\right]\\ &= \left(\frac{1}{j}\right)\left[X_{si}(\omega) - X_{si}^*(\omega)\right]\\ &\quad + \left(\frac{1}{j}\right)\left[X_{ni}(\omega) - X_{ni}^*(\omega)\right]. \end{aligned} \quad \text{(A15)}$$

Then

$$\begin{aligned}&\operatorname{Cov}\left\{J_i(\omega_1), J_r(\omega_2)\right\}\\ &= -2E\Big\{\operatorname{Re}\left[X_{si}(\omega_1)\ X_{sr}(\omega_2) - X_{si}(\omega_1)\, X_{sr}^*(\omega_2)\right]\\ &\quad + \operatorname{Re}\left[X_{ni}(\omega_1)\, X_{nr}(\omega_2) - X_{ni}(\omega_1)\, X_{nr}^*(\omega_2)\right]\Big\}. \end{aligned} \quad \text{(A16)}$$

Similar to the previous proof of (A14), we can easily show

$$E\left[f_4'^{(i)}(k_1)\, f_4'^{(r)}(k_2)\right] = G_{ir}(k_1, k_2). \quad \text{(A15)}$$

Equations (A14) and (A17) imply (A1). Next, we prove (A2).

From (A12) and (A15) we have

$$\begin{aligned}&\operatorname{Cov}\left\{I_i(\omega_1), J_r(\omega_2)\right\}\\ &= 2E\Big\{\operatorname{Im}\left[X_{si}(\omega_1)\, X_{sr}(\omega_2) - X_{si}(\omega_1)\, X_{sr}^*(\omega_2)\right]\\ &\quad + \operatorname{Im}\left[X_{ni}(\omega_1)\ X_{nr}(\omega_2) - X_{ni}(\omega_1)\, X_{nr}^*(\omega_2)\right]\Big\}\\ &\approx \frac{-2P_R}{B_S T} \operatorname{Im}\left\{\Gamma_{ir}(\omega_1 - \omega_2) \exp\left\{j\omega_2(i-r)D\right\}\right\}\\ &\quad - \frac{2b'}{T} \operatorname{Im}\left\{W_S(i-r, \omega_1 - \omega_2) \exp\left\{j\omega_2(i-r)D\right\}\right\}\\ &= \frac{-2P_R}{B_S T} \operatorname{Im}\left\{L_{ir}(\omega_1, \omega_2)\right\}. \end{aligned} \quad \text{(A18)}$$

From (A8), (A9), and (A18), one can infer that (A2) holds.

Case II: Noise-Only Case: All the proof can be applied in this case with replacing $P_R = 0$ and $W_S(q, k) = W_N(q, k)$, $M = N$. Therefore, from (A3) and (A5),

$$\begin{aligned}&G_{ir}(k_1, k_2)\\ &= \left(\frac{2^{b_1+b+d_1+d_2}}{NC_l}\right)^2 \left(\frac{b'}{2T}\right) \operatorname{Re}\left[W_N(i-r, k_1 - k_2)\right.\\ &\quad \left. \cdot \exp\left\{j2\pi k_2(i-r)D/N\right\}\right] \end{aligned}$$

which is (A6). Similarly, from (A4) and (A5), we can easily show (A7).

Appendix B
Intermediate Equations in the Design Example

For the design example described in Section V, the following equations were obtained:

$$E[h_4(k)] = E[h_4'(k)] = 0, \quad \text{for } 2 \le k \le M-2, \quad \text{(B1)}$$

$$\phi_4(k) = \phi_4'(k) = \sigma^2 \phi_W(k), \quad \text{(B2)}$$

$$\phi_W(k) = \begin{cases} 6, & k = 0; \\ -4, & k = 1, \quad M-1; \\ 1, & k = 2, \quad M-2; \\ 0, & \text{otherwise}, \end{cases} \tag{B3}$$

$$E[h_5^{(i)}(k)] = E[h_5^{\prime(i)}(k)] = \phi(0) = 6\sigma^2, \tag{B4}$$

$$\phi_5^{(i)}(k) = \phi_5^{\prime(i)}(k) = 2\phi_4^2(k) + 4\phi_4(k)\,\phi_f^{(i)}(k), \tag{B5}$$

$$\text{Cov}\left\{h_6^{(i)}(k_1), h_6^{(r)}(k_2)\right\} = \left[2^{-2l+1}\phi_5^{(i)}(k_1 - k_2) + \sigma_6^2\delta(k_1 - k_2)\right]\delta(i - r). \tag{B6}$$

Without showing tedious mathematical manipulations, we simply show the result for $E[h_7]$ and Var $[h_7]$ as follows:

$$E[h_7] = 2^{-a}\left[K_S N_{PS} k_S (2^{-l+2}3\sigma^2 + m_6)\right] + m_7 \tag{B7}$$

and

$$\begin{aligned} \text{Var}\,[h_7] = {} & N_{PS}2^{-2l-2a+3}\sigma^2 \\ & \cdot \left[\sum_{i=1}^{K_S} (35\sigma^2 + 6\phi_f^{(i)}(0) \right. \\ & - 8\phi_f^{(i)}(1) + 2\phi_f^{(i)}(2))\,k_S \\ & \left. - (18\sigma^2 - 8\phi_f^{(i)}(1) + 4\phi_f^{(i)}(2))\right] \\ & + 2^{-2a}N_{PS}K_S k_S \sigma_6^2 + \sigma_7^2 \end{aligned} \tag{B8}$$

for the signal-plus-noise case. The computation for roundoff noise-to-signal ratio V is trivial after $E[h_7]$ and Var $[h_7]$ are obtained.

Before continuing we have to determine the roundoff-dependent m_i and σ_i^2. Assume that a two's complement integer representation is used with bit truncation rather than rounding. Furthermore, assume that e_i's, for $i \neq 2$, are uniformly distributed. One can show that a truncation error e, with the uniform distribution, has mean m_e and variance σ_e^2.

$$m_e = \begin{cases} -\frac{1}{4}, & \text{if} \quad t = 1; \\ -\frac{3}{8}, & \text{if} \quad t = 2; \\ -\frac{1}{2}, & \text{if} \quad t \geq 3; \end{cases} \tag{B9}$$

and

$$\sigma_e^2 = \begin{cases} \frac{1}{16}, & \text{if} \quad t = 1; \\ \frac{5}{64}, & \text{if} \quad t = 2; \\ \frac{1}{12}, & \text{if} \quad t \geq 3; \end{cases} \tag{B10}$$

where t is the number of bits truncated. Thus, $m_i = m_e$ and $\sigma_i^2 = \sigma_e^2$ for $i = 1$, 6, and 7. The mean and variance of e_2 depend on the implementation of FFT. Assume that the FFT is implemented by decimation-in-frequency method with a bit-shifted to the right before FFT butterfly calculation. Then $m_2 = -0.5$ and $E[e_2^2 + e_2^{\prime 2}] = 2.06$ which are consistent with [7]. Therefore, $\sigma_2^2 = 1.56$ and σ^2 [see (15)] is

$$\sigma^2 = \frac{2^{2b+1}}{M}\frac{1}{12} + 1.56. \tag{B11}$$

Acknowledgment

We appreciate the valuable suggestions by one of the anonymous reviewers.

References

[1] C.-Y. Chi, D. Long, and F. Li, "Radar backscatter measurement accuracies using digital Doppler processors in spaceborne scatterometers," *IEEE Trans. Geosci. Remote Sensing*, vol. GE-24, pp. 426–437, May 1986.

[2] D. Long, C.-Y. Chi, and F. Li, "Digital filter processor design for spaceborne scatterometers," in *Proc. Int. Geosci. Remote Sensing Symp.*, Strasbourg, France, Aug. 1984.

[3] E. Braclente *et al.*, "The SASS scattering coefficient (σ_0) algorithm," *IEEE J. Ocean Eng.*, vol. OE-5, Apr.1980.

[4] R. Fisher, "Standard deviation of scatterometer measurements from space," *IEEE Trans. Geosci. Electron.*, vol. GE-10, pp. 106–113, Apr. 1972.

[5] W. L. Jones *et al.*, "The SEASAT-A satellite scatterometer: The geophysical evaluation of remotely sensed wind vectors over the ocean," *J. Geophys. Res.*, vol. 87, no. C5, pp. 3297–3317, 1982.

[6] L. C. Schroeder *et al.*, "The relationship between wind vector and normalized radar cross section used to derive SEASAT-A satellite scatterometer winds," *J. Geophys. Res.*, vol. 87, no. C5, pp. 3318–3336, Apr. 1982.

[7] T.-T. and B. Liu, "Fixed-point fast Fourier transform error analysis," *IEEE Trans. Acoust., Speech, Signal Processing*, vol. ASSP-24, Dec. 1976.

[8] A. V. Oppenheim and R. Schafer, *Digital Signal Processing*. Englewood Cliffs, NJ: Prentice-Hall, 1975.

[9] A. Papoulis, *Probability, Random Variables, and Stochastic Processes*. New York: McGraw-Hill, 1965.

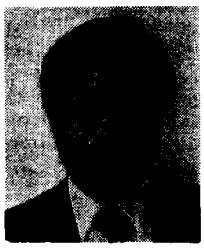

Chong-Yung Chi was born in Taiwan, Republic of China, on August 7, 1952. He received the B.S. degree from Tatung Institute of Technology, Taipei, Taiwan, in 1975, the M.S. degree from the National Taiwan University, Taipei, Taiwan, in 1977, and the Ph.D. degree from the University of Southern California, Los Angeles, in 1983, all in electrical engineering.

In September 1979 he was appointed a Teaching/Research Assistant, and later became a Research Assistant in the Department of Electrical Engineering-Systems at the University of Southern California. Since July 1983 he has been with the Jet Propulsion Laboratory at Pasadena, CA. Currently he is engaged in the studies of spaceborne radar scatterometer systems and deconvolution of radar altimeter signals. His research interests include digital signal processing, deconvolution, adaptive filtering, system identification, and estimation theory.

David Long received the B.S. degree in electrical engineering from Brigham Young University, Salt Lake City, UT, in 1982, and the M.S. degree in electrical engineering with emphasis in signal processing in 1983.

Since 1983 he has been employed at the Jet Propulsion Laboratory in Pasadena, CA, as a member of the Technical Staff in the Radar Science and Engineering Section. He is also currently pursuing the Ph.D. degree in electrical engineering (signal processing) at the University of Southern California, Los Angeles. His technical/research interests include speech and digital signal processing, multidimensional signal processing, artificial intelligence, and radar remote sensing.

Mr. Long is a member of Tau Beta Pi, Eta Kappa Nu, and Sigma Xi, and has served as Vice-Chairman of a student chapter of the IEEE.

Fuk-Kwok Li was born in Hong Kong in 1953. He received the B.Sc. and Ph.D. degrees in physics from the Massachusetts Institute of Technology, Cambridge, in 1975 and 1979, respectively.

He joined the Jet Propulsion Laboratory, California Institute of Technology, in 1979, and has been involved in the studies of spaceborne radar systems. He has developed a digital SAR processor/simulator, investigated the tradeoffs on various SAR image quality parameters, and developed several techniques for SAR Doppler parameter estimation. Since 1983 he has been involved in the design and development of ocean scatterometers. Presently he is the Supervisor of the Radar Systems Science and Engineering Group.